

Single particle cryo-electron microscopy unravels the conformational flexibility and drug susceptibility of SARS-CoV2 Spike Protein

Introduction

Severe acute respiratory syndrome coronavirus 2 (SARS-CoV2), a novel β -coronavirus of the Coronaviridae family, was first isolated in December 2019 from the Hubei province of China (Zhou et al., 2020a). Initially thought to have originated in bats, SARS-CoV2 rapidly transmitted among human hosts leading to a declaration of “public health emergency of international concern” (PHEIC) by the World Health Organisation (WHO). SARS-CoV2, so called because of its 76% shared amino acid identity with the 2002 SARS-CoV coronavirus (Ou et al., 2020), causes a severe respiratory ailment with concomitant co-morbidities. The viral pandemic is still severely afflicting mankind in the pattern of “waves of infection” and has surpassed a toll of 4.5 million lives as of September 28, 2021 (WHO Daily Report). SARS-CoV2, like other human coronaviruses, is an enveloped, positive sense RNA virus comprising a large nucleocapsid protein. The virion surface is densely populated with trimeric Spike (S) glycoproteins that render a ‘corona’ or crown-like appearance (Tortorici and Veasler, 2019). Apart from being the most characteristic feature of coronaviruses, S protein is also one of the most well studied targets for neutralizing antibody generation. The reason behind this major focus is because the S proteins form the first point of recognition with the host cells. S protein can be broadly divided into two subunits – the S1 subunit and the S2 subunit. The S2 subunit fixes the S protein to the viral membrane while the S1 subunit is involved in deploying a specific kind of receptor protein (called human Angiotensin Converting Enzyme 2 or hACE2) (Walls et al., 2020) as a gateway to enter the lungs and hijack the body functions. However, entry within the cells can only be accessed when the S protein is in ‘open’ state or when one or more of the three hinge-like domains (Receptor Binding Domains or RBD) in the S1 part is in the standing up position (Lan et al., 2020; Zhou et al., 2020b). Following viral and cellular membrane fusion, the S protein is cleaved by host cell proteases at the boundary between the S1 and S2 subunit to form the tubular, elongated post-fusion state (Xia et al., 2020).

Owing to the founder’s role played by the S protein in eliciting pathogenesis, several structural studies have been carried out to better characterize this heavily glycosylated viral structural protein. Unanimously, reports suggested the presence of distinct 1-RBD up and 3-RBD down states of trimeric S protein (Toelzer et al., 2020; Walls et al., 2020; Wrapp et al., 2020; Xiong et al., 2020; Zhou et al., 2020b). Recent cryo-electron tomography study revealed the presence of a minor 14% population of the 2-RBD up open S protein trimers on the membrane of intact virions (Ke et al., 2020). However, unless stabilized by mutations, such a 2-RBD up conformation has not been observed in purified S protein trimers (Korber et al., 2020). The flexible nature of the RBD region upon binding hACE2 and in the apo state was also indicated at acidic endosomal pH values (pH 4 – pH 5.5) (Zhou et al., 2020b). Thorough assessments of MERS-CoV and SARS-CoV S protein suggested moderate flexibility in the N-terminal domain (NTD) although, akin SARS-CoV2 S protein, the dramatic movements were restricted to the RBD region (Yuan et al., 2017).

As an immediate response to WHO’s PHEIC alarm, various FDA-approved drugs such as remdesivir, hydroxychloroquine, ritonavir, lopinavir were authorized emergency use for

symptomatic treatment of COVID-19 patients. Despite showing promising *in vitro* and *in silico* results as a potent viral entry inhibitor (Yao et al., 2020; Liu et al., 2020; Yuan et al., 2020; Ou et al., 2021; Nimgampalle et al., 2020; Eweas et al., 2021; Celik et al., 2020), the hydroxychloroquine wing of the Solidarity Trial was revoked in June 2020 due to the seemingly less improvement in the mortality rates of hospitalized patients (Repurposed Antiviral Drugs for Covid-19 — Interim WHO Solidarity Trial Results, 2021). On the other hand, consistent efforts from diverse research groups reported novel peptide inhibitors, antibodies and nanobodies to effectively target the homotrimeric S protein (Park et al., 2019; Toelzer et al., 2020; Cao et al., 2020; Bracken et al., 2021; Cerutti et al., 2021; Hanke et al., 2020; Huo et al., 2020). At the outset of the pandemic, this vast repository of structural data laid foundation for understanding SARS-CoV2 mediated viral entry. Although existing literature had given insight into the RBD movement, the precise trajectory of motion facilitating the RBD and NTD interaction with hACE2 and/or neutralizing antibodies at the physiological pH, remained unaddressed. Thus, we conceptualized a single particle cryo-electron microscopy-based study to identify the multiple phases of RBD and NTD of S protein at and near physiological pH. Our results indicated the presence of myriad conformational intermediates that have distinct structural shifts, directly altering the cavity architecture between the RBD and NTD. Moreover, we were able to show that the distribution of S trimers at physiological pH 7.4 assumes a predominantly open (or receptor-accessible) state as compared to a slightly acidic or alkaline pH (Pramanick et al., 2021). We further characterized the role of 1-RBD up S protein structural state at pH 7.4 by treating with a known viral entry inhibitor drug as well as a novel peptide molecule. Interestingly, we observed drug induced aggregation of S protein and peptide induced S protein dimer formation, both of which hamper interaction with hACE2 receptor. Thus, extensive characterization of the conformational flexibility and inhibitor driven structural alterations will help enrich existing knowledge and inform vaccine and therapeutic design.

Objectives

1. To resolve high resolution structures of S protein at physiological pH (pH 7.4) and near-physiological pH (pH 6.5 and pH 8.0).
2. Identification of the intermediate populations of 1-RBD up open and 3-RBD down closed states of S protein.
3. To assess the biological significance of NTD and RBD flexibility on the interaction of S protein with neutralizing antibodies and hACE2.
4. Identification of the glycosylation sites which render immune protection to SARS-CoV2 against host defense mechanism.
5. Characterization of the impact of drugs and peptide inhibitors on the structural stability of SARS-CoV2 S protein.

Methods:

Expression and Purification of S protein:

S-2P, an S protein construct with two proline mutations at the residues 986 and 987 in the S2 subunit, was synthesized (Genscript, USA) with expression was carried out under the control of a CMV promoter through mammalian cell culture (Expi293F Cells, Gibco, Thermo Fisher). Transfection was performed (ExpiFectamine 293 Transfection kit, Gibco) according to the manufacturer's protocol. This was followed by collection of culture supernatant from transfected cells after 5 days. S-2P was subsequently purified by immobilized metal affinity chromatography using Ni-Sepharose 6 Fast flow resin (G-Biosciences). Ni-NTA beads were first equilibrated with PBS (pH 7.4), followed by incubation with the culture supernatant in the presence of 1 mM PMSF (Sigma Aldrich). Protein was eluted using a concentration gradient of Imidazole (200 mM-500 mM), and then dialyzed against PBS (pH 7.4). His-Tag was cleaved using HRV-3C protease cleavage. For cryo-EM grid freezing, S protein was dialyzed with 25 mM Tris and concentrated with 100 kDa centrifugal filter unit (Amicon).

Expression and purification of ACE2-hFc:

The plasmid pCD5-mACE2-T-Fc was a kind gift from Dr. Neil King, University of Washington. Macaque ACE2 ectodomain gene was fused to a sequence encoding thrombin cleavage site and human Fc fragment. The whole sequence was amplified and introduced in pCDNA3.4 plasmid with CMV promoter. Expi293F cells (Gibco, ThermoFisher) were transiently transfected with pCD5-mACE2-T-Fc plasmid as per manufacturer's protocol. Culture supernatant was harvested 5 days after transfection using centrifugation. Protein was purified by IMAC using Protein G Sepharose 4 Fast flow resin (GE Healthcare). The column was pre-equilibrated using 1x PBS (pH 7.4). Elution of the protein was carried out with 0.1 M Glycine-HCl (pH 2.5) and neutralized by 1 M Tris-HCl (pH 9.0). The eluted protein was dialyzed twice against 1x PBS (pH 7.4).

Sample preparation for Negative Staining Transmission Electron Microscopy (NS-TEM):

Homogeneity and spatial distribution of S protein samples at three different pH conditions (pH 6.5, pH 7.4, and pH 8.0) was directly analyzed using NS-TEM. S protein (pH 7.4) was also separately incubated with hACE2, linoleic acid and Drug A for 20 minutes at room temperature prior to NS-TEM analysis. 3.5 μ l of each sample (0.1 mg/ml) was added to glow-discharged carbon coated Cu grid (300 mesh, EMS) and incubated for 90 seconds. Excess sample was blotted, and the film was negatively stained using 1% uranyl acetate. Data acquisition was performed using 120 kV Tecnai T12 electron microscope with side-mounted Olympus VELITA CCD camera (2k x 2k) and 120 kV Talos L120C transmission electron microscope (ThermoFisher) equipped with Ceta (4k x 4k) camera. Calibrated pixel size was 2.96 Å/pixel.

Image Processing for NS-TEM:

For all samples, particles were manually picked in EMAN 2.1 (Tang et al., 2007) and then extracted using e2boxer.py in EMAN 2.1. Reference free 2D classifications were calculated first in RELION 2.0 (Scheres, 2012) to select best 2D classes, and subsequently in SIMPLE 2.0 using simple simple_prime2D (Elmlund and Elmlund, 2012).

Sample preparation and data acquisition for cryo-Electron Microscopy (cryo-EM):

3 μ l of each protein sample (pH 6.5, pH 7.4, and pH 8.0) and reaction mixtures (S protein and Drug A in 1:1 ratio) were applied on glow discharged Quantifoil R1.2/1.3 300 mesh gold grids and incubated at room temperature and 100% humidity for 10 sec. Excess sample was blotted out for 8 seconds, followed by rapid plunging into liquid ethane using FEI Vitrobot Mark IV. Data was acquired at 42200x magnification (pixel size at specimen level: 1.17 Å/pixel) under Thermo Scientific™ 200 kV Talos Arctica Transmission Electron Microscope equipped with K2 Summit Direct Electron Detector (Gatan Inc). Automatic data collection was performed using LatitudeS (Gatan Inc.). A total of 20 frames was acquired per movie with a total calibrated dose of 80 e-/Å², with defocus ranging between -0.75 to -2.5 μ m.

A total of 2405, 4504 and 3166 movies were acquired for S protein at pH 8.0, pH 7.4 and pH 6.5, respectively. Around 5292 movies were collected for S protein treated with Drug A in molar ratio 1:1.

Cryo-EM Image Processing:

Initially, the acquired movies were imported into RELION 3.0 and corrected for beam-induced motion using MotionCor2 (Li et al., 2013) software, and the resulting micrographs were then screened in cisTEM (Grant et al., 2018). The best micrographs were considered for further processing. CTFFIND 4.1.13 (Rohou and Grigorieff, 2015) was used to estimate contrast transfer function for these micrographs. A subset of particles was first manually picked and then subjected to reference free 2D classification to yield good 2D class averages for template-based auto-picking of particles. The automatically picked particles were extracted with a box size of 256 pixels, and several rounds of reference free 2D classification was performed to remove broken and false particles. Around 10 percent of particles were selected for generation of a model *ab-initio*. Finally, about 330, 534 (pH 6.5), 723,229 (pH 7.4), 303,194 (pH 8.0), and 865,506 (S protein treated with Drug A) particles were selected for 3D classification without imposition of any symmetry (C1 symmetry). Auto-refinement was carried out for classes with high-resolution features for all datasets. This was followed by CTF refinement and Bayesian polishing, and one final round of 3D auto-refinement with polished particles using RELION 3.0.

The auto-refined maps were sharpened in RELION 3.0 and PHENIX (Adams et al., 2010). Fourier shell correlation (FSC) were estimated for all the high-resolution maps at 0.143, and local resolution estimation using unfiltered refined maps was performed within ResMap (Kucukelbir et al., 2014).

Real space refinement and structure assessment using cryo-EM density maps:

The sharpened maps were docked with 1 RBD up (PDBID: 6vyb) and 3 RBD down (PDBID:6zwv) and real space refinement of the docked model with respect to the cryo-EM maps was performed using phenix.real_space_refine in PHENIX. The resultant real space refined models were further used for structure assessment. EMRinger (Barad et al., 2015) score was calculated for each cryo-EM map using PHENIX. RMSD between atomic models corresponding to different conformational states (aligning C α) was estimated using PyMOL (The PyMOL Molecular Graphics System, Version 1.2r3pre, Schrödinger, LLC.). Solvent Accessible Surface Area (SASA) of key amino acid residues was also calculated for each conformer using NACCESS (Hubbard, S.J. and Thornton, 1993). All structural analyses were

performed using UCSF Chimera (Pettersen et al., 2004) and UCSF ChimeraX (Goddard et al., 2018).

Results

SARS-CoV2 S protein is a dimorphic protein which exists in a kinetically stable prefusion state before viral membrane fusion with the host cell membrane (Kirchdoerfer et al., 2016). Following adherence to host cell surface receptor hACE2, the prefusion state S protein is cleaved at a specific RRAR site at the S1/S2 boundary by ubiquitously present host furin proteases (Xia et al., 2020). Since the outbreak of the pandemic, several high resolution cryo-EM structures of S protein were solved at pH 8.0 to understand the overall structure of the S protein (Wrapp et al., 2020; Walls et al., 2020; Henderson et al., 2020; Toelzer et al., 2020). Additionally, studies reported the variability of the RBD region between the apo state and hACE2 receptor bound state at a range of endosomal pH (Zhou et al., 2020b). Therefore, we designed a study to monitor the effect of pH on the structural distribution of apo S protein at physiological pH (pH 7.4) and near physiological pH (pH 6.5 and pH 8.0) through single-particle cryo-EM (Pramanick et al., 2021). Initially the freshly purified S protein trimers at the three different pH values were screened for overall sample homogeneity using negative staining transmission electron microscopy (NS-TEM). The TEM revealed uniform distribution of cone-shaped trimers at all three physiologically relevant pH values – pH 6.5, pH 7.4 and pH 8.0. Based on the monodispersed nature of the protein particles on the TEM grids, we proceeded ahead with cryo-EM analysis of S protein at and near physiological pH. The unique sample preparation technique of cryo-EM, which involves very rapid freezing (called plunge freezing) of the biological sample in liquid ethane cooled by ambient liquid nitrogen, preserves the native state of the sample. Therefore, we chose to characterize the pH dependent changes in S protein with cryo-EM to obtain a more biologically native representation.

The S protein trimers were uniformly distributed at cryogenic temperature at three pH values. At first, we performed 3D reconstruction of S protein at pH 8.0. In accordance with previously reported structures, the S protein displayed a stable trimeric S2 subunit and a flexible asymmetric S1 region. Therefore, we performed 3D classification with the entire dataset without imposing any symmetry to obtain the open-close ratio at pH 8.0. The maximum likelihood-based 3D classification approach assisted us to identify internal flexibility and dynamics of biological macromolecules. The 3D classification of this dataset suggested that the overall trend was in favour of a more closed structural form of S protein with 61% of the population in a 3-RBD down closed state and 39% in a 1-RBD up open state. However, as till then most structural studies were performed at pH 8.0, we focused more on the structural states at pH 7.4 and pH 6.5. To address the plausible existence of conformational variability and intermediate states of open and closed RBD, we performed robust 3D classification to split the dataset. Through initial data processing and particle curation, we obtained 723,229 S protein particles which were then classified into 15 classes using C1 symmetry. Our 3D reconstructions revealed multiple phases of 1-RBD up open and 3-RBD down closed structures of S protein at physiological pH. Interestingly, we were also able to report the flexible nature of the NTD. Following the same pipeline of particle curation and extensive 3D classification for the study at pH 6.5, we obtained several distinct high resolution structural states of S protein. The best

maps for both the pH studies were considered for real-space refinement to obtain information at the atomic level, which could help pin-point the variability observed in the RBD and NTD regions. At pH 7.4, we obtained two high resolution maps for closed state and two high resolutions maps for the open state. Comparison of the atomic models of the 3-RBD down closed maps revealed that the RBD regions of both the maps were shifted from each other by nearly 8 Å. Similarly, the NTD of both the maps also showed remarkable flexibility by being displaced from each other by 10 Å. However, the entire structural variability was restricted to the RBD and NTD harbouring S1 region of the 3-RBD down closed S protein conformations. In contrast, the alignment of the atomic models of 1-RBD up open S protein at physiological revealed an unexpected shift of more than 11 Å at the membrane proximal non-helical part of the S2 region. However, the respective structural variations in the RBD and NTD were restricted to ~ 6 Å. This lead to only a nominal increase in the size of the cavity lining the NTD and the RBD region. The most noteworthy aspect of our study at pH 7.4 was the revelation that as high as 68% of the S trimers existed in the 1-RBD open state as compared to pH 8.0. This result indicated that physiological pH provides an environment more conducive to RBD-hACE2 interaction which could imply higher viral entry rates at physiological pH than at the previous pH conditions studied.

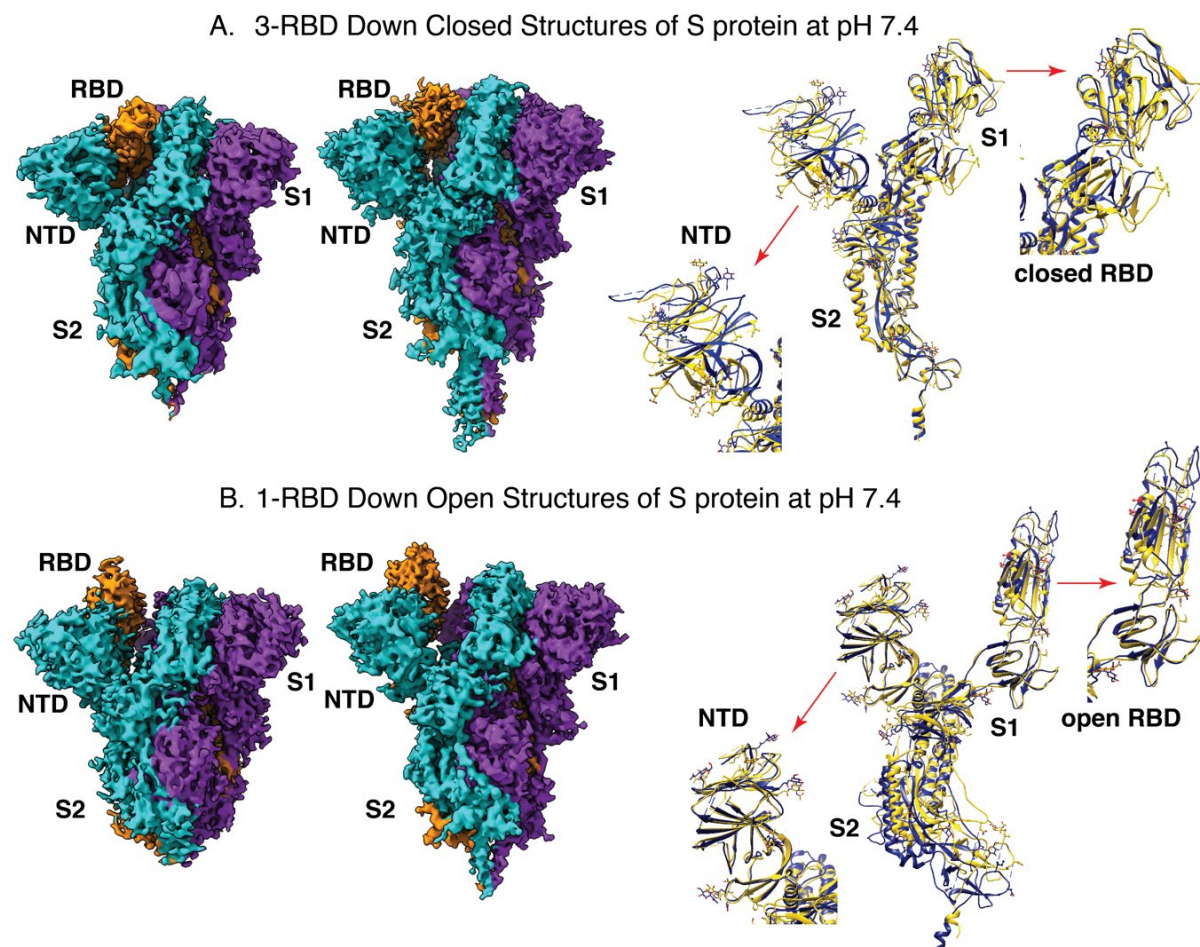


Figure 1 : (A) shows the cryo-EM density maps of 3-RBD down closed structures of S protein at pH 7.4 and the alignment of the respective atomic models showing variability in the RBD and the NTD region. (B) shows the cryo-EM density maps of 1-RBD up open structures of S protein at pH 7.4 and the alignment of the respective atomic models showing variability in the RBD and the NTD region.

To obtain a holistic picture of the trend of variability, we proceeded to analyse the structural states at the acidic end of near-physiological pH, pH 6.5. The high resolution maps were taken further for real space refinement. Remarkably, aligning the closed models revealed different extents of packing of the RBD, thereby providing us a loosely packed closed state and a compact closed state of S protein at pH 6.5. Although the S2 regions of the two 3-RBD down states showed close correlation, the S1 region showed impressive flexibility where the NTD and RBD regions were displaced in the range of ~ 7.5 Å and ~ 7 Å, respectively. Similarly, alignment of the open state S protein maps also revealed significant displacements in the open RBD and NTD region.

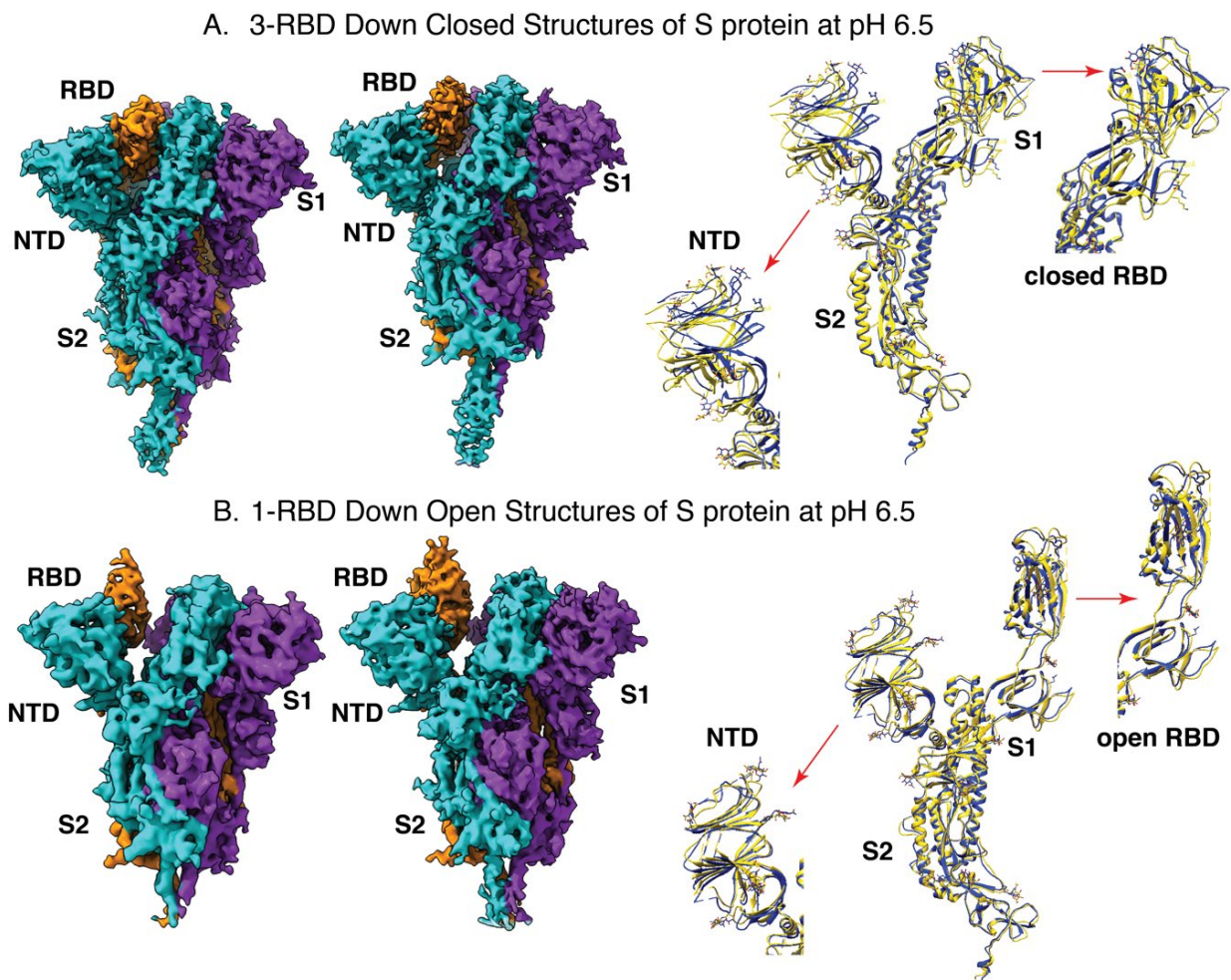
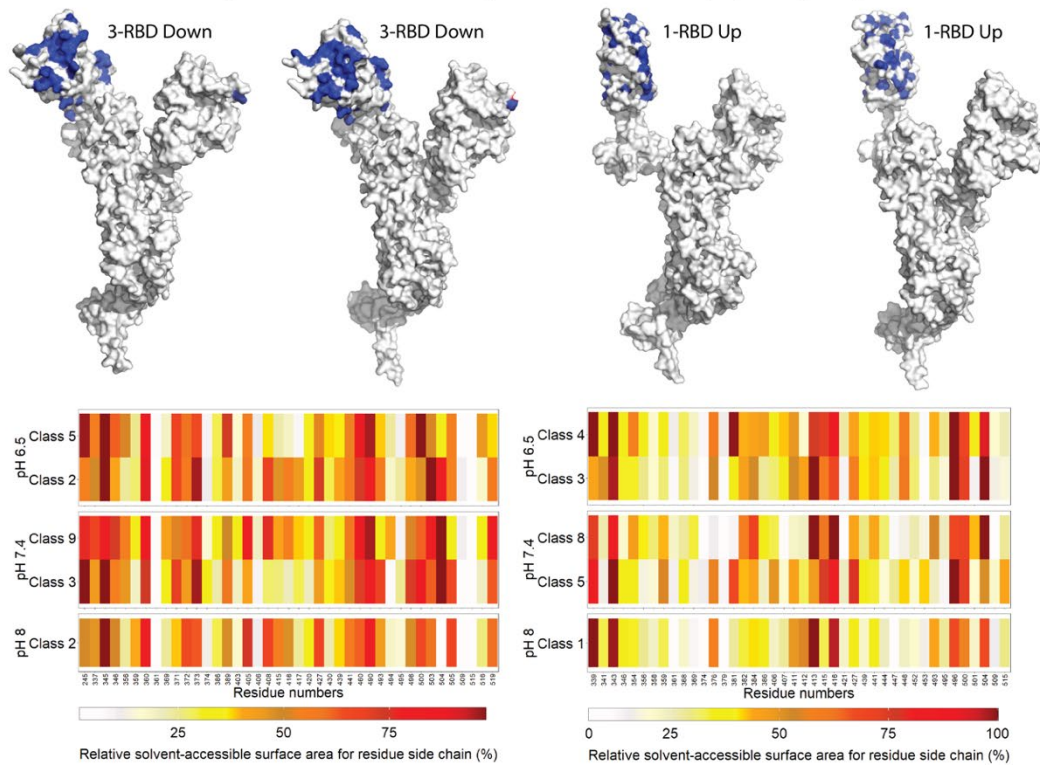


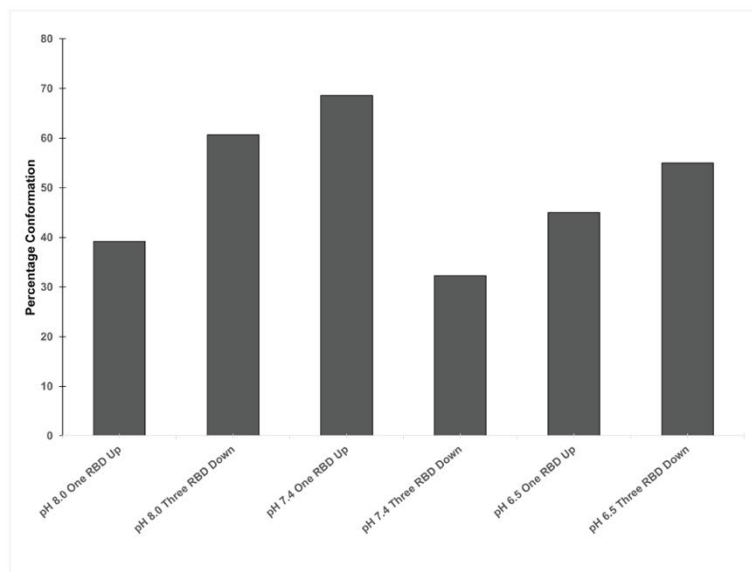
Figure 2 : (A) shows the cryo-EM density maps of 3-RBD down closed structures of S protein at pH 6.5 and the alignment of the respective atomic models showing variability in the RBD and the NTD region. (B) shows the cryo-EM density maps of 1-RBD up open structures of S protein at pH 6.5 and the alignment of the respective atomic models showing variability in the RBD and the NTD region.

Analysis of the structural disposition of S protein revealed that nearly 50% of the S proteins assumed a 1-RBD up state. This showed that only at physiological pH, pH 7.4, S protein exists as predominantly open form, while on both the acidic and alkaline side of the pH scale, the closed conformers are favoured. Obtaining a milieu of open and closed forms at the three pH values led us to ask the next relevant question – what is the biological significance of the intermediate structures? To address the query, we calculated the solvent accessible surface area of the high resolution 1-RBD up and 3-RBD down structures obtained at different pH conditions. Interestingly, we observed nearly 40 key amino acid residues, which were previously shown to engage different neutralising antibodies and hACE2 receptor, showed varied extents of solvent exposure. This could indicate that inherent flexibility of the S1 region of S protein facilitates elicitation of epitopes which are otherwise buried in closed conformation. Along with the flexible nature of the RBD, the pathogenic success of SARS-CoV2 can also be attributed to the extensive glycosylation which makes the virus “invisible” to host immune cells. Therefore, to obtain more structural information, we imposed C3 symmetry on the pH 7.4 dataset and obtained a 3.9 Å closed map of S protein. In this high resolution reconstruction, we were able to identify 18 N-linked and 1 O-linked glycosylation sites out of the 23 predicted total glycosylation sites. Thus our map clearly revealed at least 19 out of 23 sites which protect the SARS-CoV2 virion against the host defense mechanism.

A. Relative solvent exposed surface area of S protein at and near physiological pH



B. Distribution of open and closed state conformations



C. Glycosylation sites in S protein

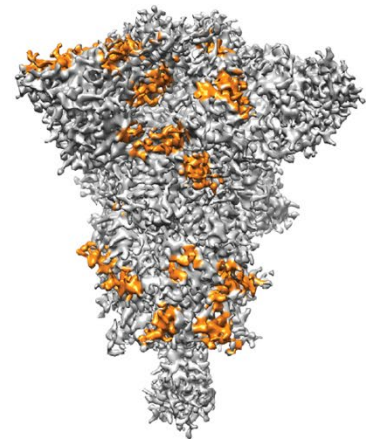


Figure 3 : (A) Top panel shows monomers of the different closed and open maps of S protein at pH 7.4. The amino acid residues which differ in SASA values are coloured blue. Bottom panel represents the heatmaps which compare the variability in solvent exposure of S protein intermediates across the three pH values. (B) Bar diagram showing the distribution of open and closed population of S protein at and near physiological pH. (C) High resolution 3-RBD down closed map of S protein (pH 7.4) shows the glycosylation sites marked in orange.

Finally, having characterised the structural behaviour of apo S protein at physiological conditions, we wanted to explore the impact of a known FDA-approved drug and a novel peptide inhibitor (data not shown, Manuscript under preparation) on the structural stability of S protein. It is a well-known fact that S protein initiates the infection cascade of SARS-CoV2 by mediating viral entry. Therefore, we thought of investigating whether a drug, say Drug A (Manuscript under communication), which is known to abrogate viral entry and has previously shown potential to prevent SARS-CoV2 entry into the host cells, had any structural basis for action. We hypothesised that since S protein plays such a pivotal role in viral entry, it is possible that Drug A may also have an effect on this structural protein to show its efficacy. Thus, we incubated freshly purified S protein with Drug A at different molar ratios. For visual inspection of any possible changes, we performed negative staining of the complexes. Surprisingly, we observed massive stretches of aggregation which increased with the increase in concentration of Drug A. This kind of aggregation was neither observed in the control S protein sample, nor was it observed in our previous pH based study when we imaged S protein at pH 6.5, 7.4 and 8.0. To test the specificity of this observation, we incubated S protein with 50 μ M linoleic acid, which has been shown to bind S protein. Remarkably, no such aggregation or network was observed at concentrations even as high as 50 μ M, whereas only 6 μ M Drug A was sufficient to favour aggregation of S protein. Moreover, it was interesting to note that even in the native condition provided by cryo-EM, this pattern of obtaining large areas of aggregated S protein was retained.

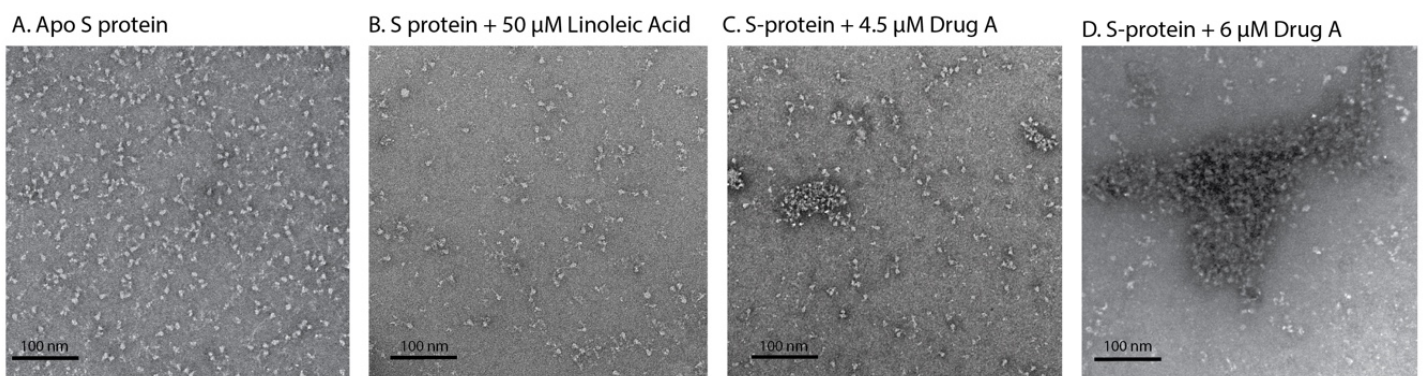


Figure 4 : (A) Negative staining raw micrograph shows uniformly distributed particles of apo-S protein. (B) Negative staining raw micrograph shows S protein treated with known ligand linoleic acid. (C) Appearance of aggregation on treating S protein with low concentration of Drug A. (D) Increase in aggregation observed on treating S protein with higher concentration of Drug A.

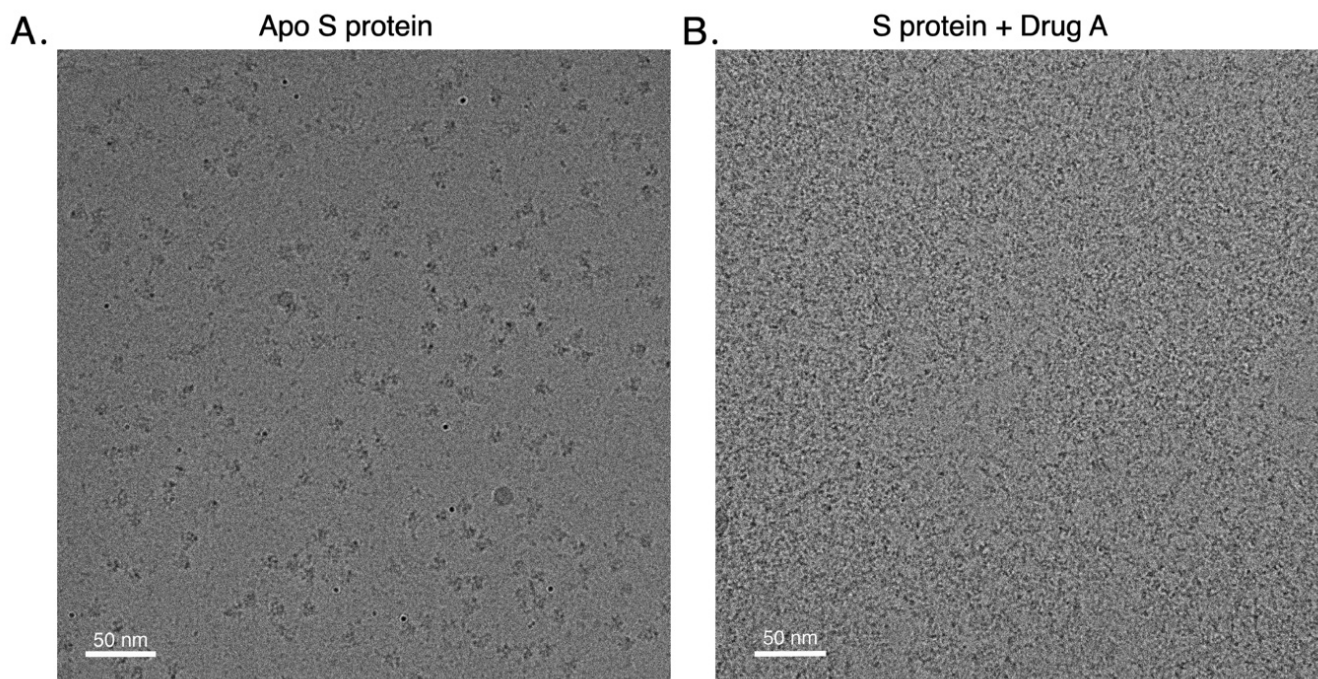


Figure 5 : (A) Cryo-EM raw micrograph shows homogenous distribution of S protein particles. (B) Cryo-EM raw micrograph shows aggregation of the same S protein sample on treatment with Drug A.

This destabilizing effect of Drug A on the free S protein molecules, made it extremely difficult for us to resolve the structure of drug bound S protein through cryo-EM. At low concentration of Drug A, $\sim 3 \mu\text{M}$, many free S proteins were observed. Although we were not able to identify the drug density in the open or closed map obtained from the drug treated dataset, it was noteworthy to find that the percentage of 1-RBD up open conformation decreased from $\sim 68\%$ in the apo state to $\sim 50\%$ in the drug treated condition. Moreover, a significant amount of S protein particles was uncharacterized due to low resolution (probably due to the destabilizing nature of Drug A) and therefore we classified them as neither open nor closed, but “unassigned” state. Upon incubating S protein and hACE2 with Drug A, we observed many free S protein and free receptor particles, which indicated hampered interaction in the presence of Drug A - a possible mechanism of Drug A to prevent SARS-CoV2 entry within host cells.

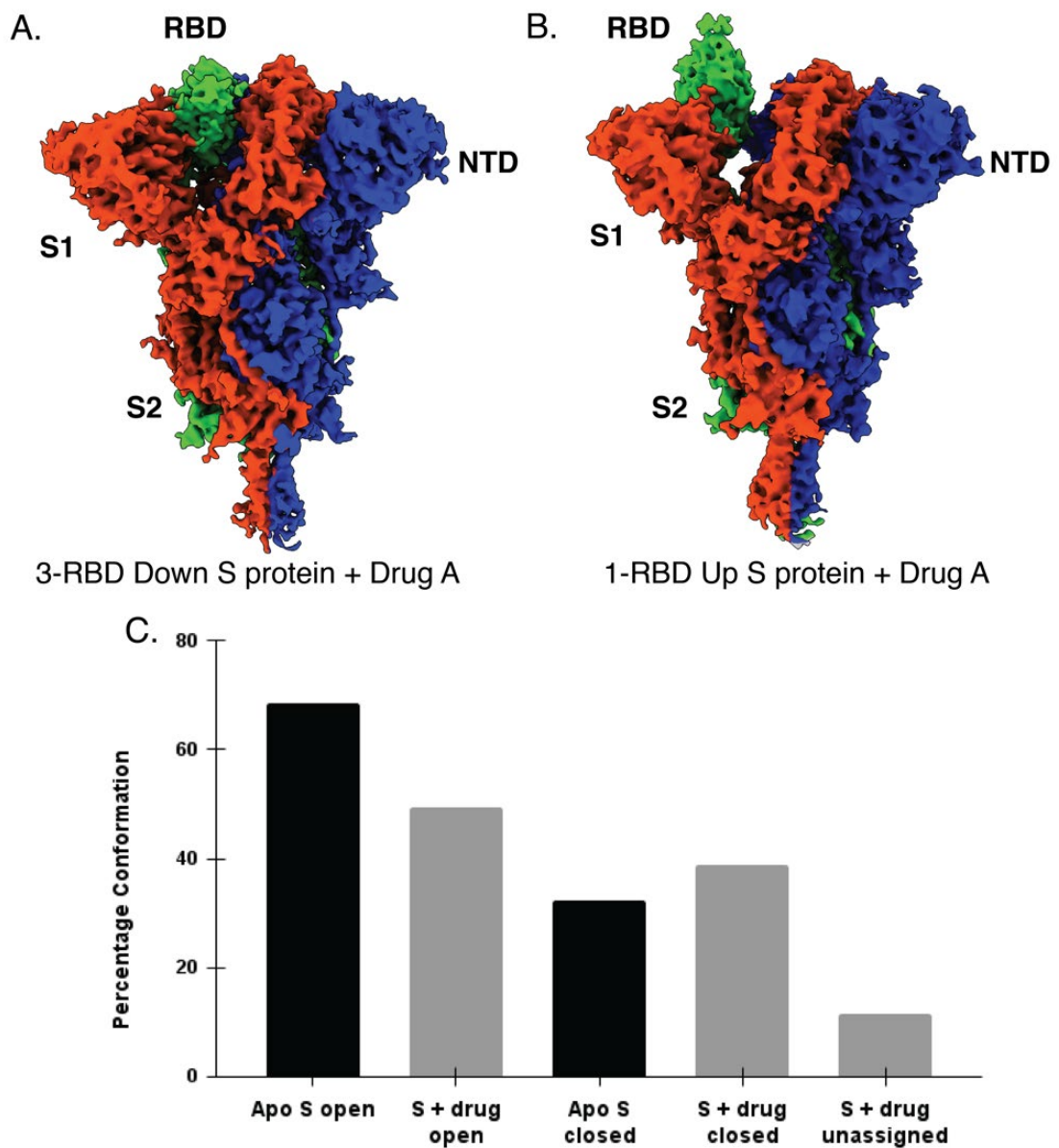


Figure 6 : (A) Cryo-EM reconstruction of 3-RBD down closed structure of S protein treated with Drug A. (B) Cryo-EM reconstruction of 1-RBD up open structure of S protein treated with Drug A. (C) Bar diagram showing the comparison of open and closed distribution of S protein with and without treatment with Drug A.

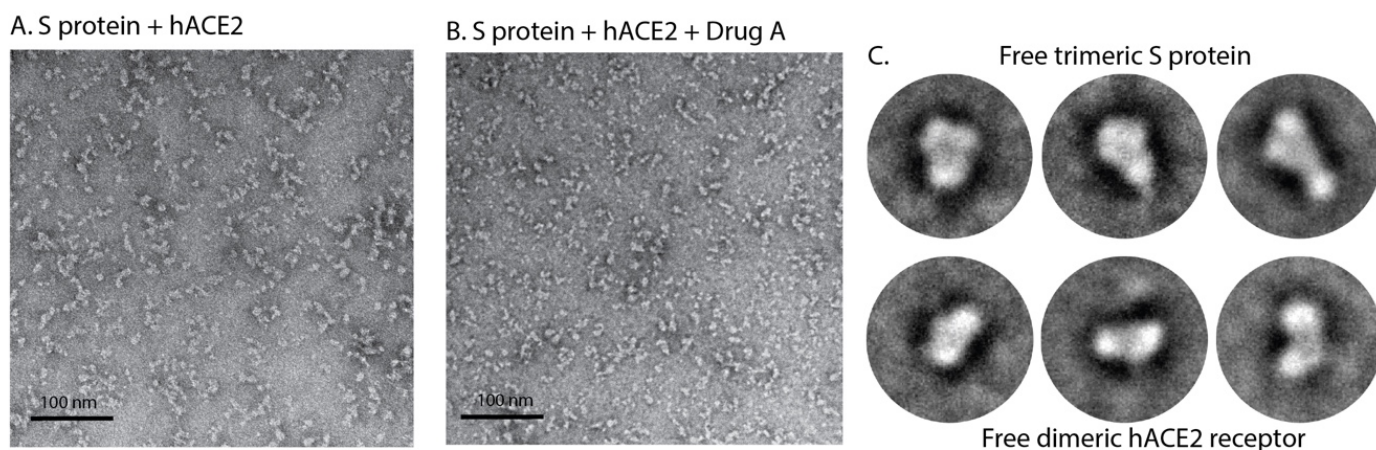


Figure 7 : (A) Negative staining raw micrograph of S protein incubated with hACE2 receptor shows elongated particles corresponding to S-hACE2 complexes. (B) Negative staining raw micrograph of S protein incubated with hACE2 in the presence of Drug A shows many free S protein particles and free hACE2 dimers. (C) 2D class averages calculated from the dataset reveals trimeric unreacted S protein particles and dimeric unreacted hACE2 dimers.

Statistical analysis

The cryo-EM image reconstruction was performed in RELION 3.0, which classifies particle images based on Maximum Likelihood Estimation (MLE). The ML approach was applied in the 2D classification and 3D classification steps to estimate the population of S protein in open and closed states. Real-space fitting of the atomic models of S protein into the individual density maps was performed by gradient-driven minimisation of the models in PHENIX `real_space_refine` program. The side chain fitting was estimated in EMRinger which determines the statistical significance of the result through a Z-score based metric over the square root of the number of amino acid residues. The structural rearrangements in the various intermediate models were studied by calculating the Root Mean Square Deviation (RMSD) value by aligning the C α of amino acid residues in PyMOL. Finally, through the Rolling Ball Algorithm applied in NACCESS program, the solvent exposed surface area was calculated in high resolution density maps.

Discussion

The SARS-CoV2 virion surface glycoprotein, the S protein, serves as an essential candidate to inform vaccine development and all the approved vaccines so far have implemented S protein constructs to provide immune protection. Since the outset of the pandemic, several studies on the S protein have reported the presence of two distinct conformations of the S protein – 1-RBD up open conformation and 3-RBD down closed conformation. The open state of the RBD is essential for hACE2 receptor engagement. An insightful study by Zhou et al focusing on the interaction of S protein and hACE2 at highly acidic endosomal pH conditions, showed that at pH 4.0, the entire population of S protein prefusion state trimers assume all RBD down conformation where hACE2 interaction is not possible (Zhou et al., 2020b). They also proposed

that hACE2 binding induces rearrangement in the RBD involved in the interacting complex. These raised some important questions – what is the distribution of S protein conformations at physiological pH? Is there any possible role of pH in governing the movement of the RBD? How flexible are the RBD and NTD of the SARS-CoV2 S protein? Are there any intermediate states of S protein at physiologically relevant conditions? In an attempt to answer these questions, we have thus, pooled the structural states of S proteins at and near physiological pH, pH 6.5, pH 7.4 and pH 8.0. From our study, we showed that nearly 68% of the total population of S trimers at physiological pH assume a receptor accessible open state. On either side of the pH scale, there was a significant decrease in the amount of open conformations, making one speculate the possibility of a pH mediated switch governing the open-close equilibrium of SARS-CoV2 S protein at physiological conditions. This hypothesis could be supported by a report suggesting that D830, D839, D843, and D848 and a disulfide bond between C840 and C851 undergo a pH-induced protonated/deprotonated switch which controls the open-close transition at endosomal pH (Zhou et al., 2020b). Interestingly, at the same time, through computational study it was proposed that the pKa of D398, which is strongly dependent on the ambient pH, determines the mobility of the RBD towards or away from the S protein core (Warwicker, 2020). Our robust particle sorting procedure based on Maximum Likelihood Estimations, also revealed multiple phases of the distinct 1-RBD up and 3-RBD down closed states. Close inspection of the structural entities pinpointed the NTD and the RBD as the most flexible parts of the S protein. It was observed that within the same pH and across mild fluctuations of pH, the packing of amino acid residues in the RBD and the NTD of these various “intermediates” were remarkably altered leading to their differential exposure to the solvent environment. It is tempting to note that among the amino acids observed to be undergoing these structural rearrangements, nearly 40 residues have been previously documented to be involved in either interacting with the hACE2 or broadly neutralising antibodies. Thus, we propose that the continuous flexibility and rearrangements in the RBD and NTD regions may influence the extent of interactions of antibodies targeted against the open or closed S proteins. To summarise, characterisation of various intermediate conformations, structural rearrangements and the predominance of 1-RBD up open state of S protein at physiological pH are the key highlights of our pH based study. The differential exposure of amino acid residues and the high proportion of open states of RBD help explain why broadly neutralising antibodies are elicited against epitopes that are buried in closed conformations.

To further probe the role of S protein in the disease pathway, we studied the effect of an FDA-approved drug which has also shown promising role as a viral entry inhibitor. The myriad conformational states of S protein at physiological pH are majorly predisposed to engage hACE2 receptor and enable viral membrane fusion with the host cells. Thus, we aimed at assessing the response of the diverse conformations to a potent viral entry inhibitor drug, Drug A. Intriguingly, we observed that S protein trimers assembled in the form of large aggregates with increasing concentration of Drug A. The observation remained unaltered at both NS-TEM and cryo-TEM conditions. As a direct comparison with apo S protein, we observed that the treatment with Drug A reduced the receptor binding potency. This was supported by the cryo-TEM data where the population of 1-RBD up open forms reduced from ~68% to ~50%, as well as by our NS-TEM data that clearly showed the appearance of free S protein particles and free

hACE2 particles when they were made to interact in the presence of Drug A. On the contrary, incubation of hACE2 with S protein at pH 7.4 amounted to the formation of large complexes, possibly due to the favourable environment of S-hACE2 interaction. Therefore, it could be proposed that the plausible cause for observing viral entry inhibition on the application of Drug A may be because of its destabilising action on S protein which hinders binding to the hACE2 receptor. However, extensive *in vivo* setting characterisations are required to comment conclusively on the protective efficacy of Drug A.

Impact of the research in the advancement of knowledge or benefit to mankind

The first case of the novel SARS-CoV2 virus was reported in end of December 2019 in Wuhan, China. Despite the sudden unexpected outbreak of this deadly virus, the scientific community provided the first studies on S protein starting as early as March 2020, which was within three months of the first reported case. Therefore, scientists all over the world had prioritised work on SARS-CoV2 and all elements were being covered which could help in the development of the vaccines which are now being successfully administered in almost every household. Initially the proteins were studied at laboratory conditions to provide the founder's knowledge. To add to the initial knowledge, we designed a study in the physiological conditions. Our experiments can be classified into two kinds – the fundamental aspect which provides mechanistic insights into the flexibility of S protein and the application based aspect where we report the morphological aberrations in S protein under the influence of a drug molecule.

According to the WHO database, most current vaccines that use whole or part of the Spike protein to elicit the production of antibodies in our bodies, have been seen to be imparting protection against most incidences of Covid-19 infection. However, one of the trademark features of RNA viruses is their rapid mutation ability. Despite having successful vaccination attempts of the worldwide population, the persistent emergence of “variant” strains of the virus is a matter of grave concern. WHO has divided these mutants in the category of Variants of Interest (VOI) and Variants of Concern (VOC) based on their rate of transmission and evasion of neutralizing antibodies. Currently, the alpha, beta, delta and gamma variants belong to VOC category of SARS-CoV2. Each of these variants show increased transmissibility, as high as 50%, and reduced susceptibility to antiviral drugs and post-vaccination sera. Multiple substitution mutations acquired by the VOC result in failure of diagnosis at early stage of infection leading to increased hospitalization and mortality rates. These mutations, most commonly D614G, N501Y, impact the S protein and hACE2 interaction. D614G mutants show the existence of 1-RBD, 2-RBD as well as 3-RBD up states with almost 95% open conformation. The predominance of the open conformation of S protein determines the increased infectivity of the virus. On the other hand, N501Y, although does not show significant structural changes but the substitution mutation increases S protein affinity for hACE2 receptor. The predicted third wave in India is thought to be caused by the delta variant which harbors new mutations along with DG14G, N501Y, such as L452R, T478K, D950N. Probing the structural impact these mutations could have on the S protein may provide insight into development of therapeutic strategies. Our study which was carried out in the middle of 2020, was the first of its kind to report the intermediate conformations, residue level

rearrangement in different intermediates and the predominance of open structures at physiological pH. Therefore, we believe that addressing the inherently flexible nature of the RBD and examining the specific residues which vary in the solvent exposure can help understand or predict the kind of mutation which the virus may undergo to improve hijacking hACE2 receptors. Cryo-electron microscopic (cryo-EM) analysis and structure determination of the mutant S protein has the potential to provide residue level information outlining the changes that increase fatality of VOC infection. Therefore, designing future studies on the objective of delineating the RBD motion and residue exposure for mutant S protein may potentially aid in the development of neutralising antibodies which are more effective against the novel mutants of SARS-CoV2.

Our ongoing application based study of S protein-inhibitor interactions provides some novel insights into the behaviour of S protein. Till date, there are no reports of any synthetic compounds which can destabilise and cause huge stretches of aggregation in S protein. Although studies have reported the formation of rosette-like structures (Li et al., 2006). Recently, these S protein rosettes are being actively pursued to develop novel therapeutic compounds and alternative vaccines. Therefore, our current work will provide a new outlook on the impact of drug treatment on viral entry abrogation. We hope that our findings will provide a foundation to pharmaceutical companies for the development of more potent analogues with least toxicity.

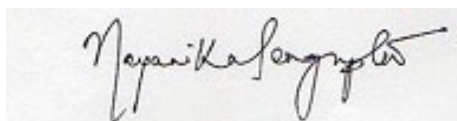
Literature references

- Adams, P.D., P. V. Afonine, G. Bunkóczi, V.B. Chen, I.W. Davis, N. Echols, J.J. Headd, L.-W. Hung, G.J. Kapral, R.W. Grosse-Kunstleve, A.J. McCoy, N.W. Moriarty, R. Oeffner, R.J. Read, D.C. Richardson, J.S. Richardson, T.C. Terwilliger, and P.H. Zwart. 2010. PHENIX : a comprehensive Python-based system for macromolecular structure solution. *Acta Crystallogr. Sect. D Biol. Crystallogr.* 66:213–221. doi:10.1107/S0907444909052925.
- Barad, B.A., N. Echols, R.Y.-R. Wang, Y. Cheng, F. DiMaio, P.D. Adams, and J.S. Fraser. 2015. EMRinger: side chain-directed model and map validation for 3D cryo-electron microscopy. *Nat. Methods.* 12:943–946. doi:10.1038/nmeth.3541.
- Bracken, C.J., S.A. Lim, P. Solomon, N.J. Rettko, D.P. Nguyen, B.S. Zha, K. Schaefer, J.R. Byrnes, J. Zhou, I. Lui, J. Liu, K. Pance, X.X. Zhou, K.K. Leung, and J.A. Wells. 2021. Bi-paratopic and multivalent VH domains block ACE2 binding and neutralize SARS-CoV-2. *Nat. Chem. Biol.* 17:113–121. doi:10.1038/s41589-020-00679-1.
- Cao, L., I. Goresnik, B. Coventry, J.B. Case, L. Miller, L. Kozodoy, R.E. Chen, L. Carter, A.C. Walls, Y.-J. Park, E.-M. Strauch, L. Stewart, M.S. Diamond, D. Veessler, and D. Baker. 2020. De novo design of picomolar SARS-CoV-2 miniprotein inhibitors. *Science (80-.).* 370:426–431. doi:10.1126/science.abd9909.
- Celik, I., A. Onay-Besikci, and G. Ayhan-Kilcigil. 2020. Approach to the mechanism of action of hydroxychloroquine on SARS-CoV-2: a molecular docking study. *J. Biomol. Struct. Dyn.* 1–7. doi:10.1080/07391102.2020.1792993.
- Cerutti, G., Y. Guo, T. Zhou, J. Gorman, M. Lee, M. Rapp, E.R. Reddem, J. Yu, F. Bahna, J. Bimela, Y. Huang, P.S. Katsamba, L. Liu, M.S. Nair, R. Rawi, A.S. Olia, P. Wang, B. Zhang, G.-Y. Chuang, D.D. Ho, Z. Sheng, P.D. Kwong, and L. Shapiro. 2021. Potent SARS-CoV-2 neutralizing antibodies directed against spike N-terminal domain target a

- single supersite. *Cell Host Microbe*. 29:819-833.e7. doi:10.1016/j.chom.2021.03.005.
- Elmlund, D., and H. Elmlund. 2012. SIMPLE: Software for ab initio reconstruction of heterogeneous single-particles. *J. Struct. Biol.* 180:420–427. doi:10.1016/j.jsb.2012.07.010.
- Eweas, A.F., A.A. Alhossary, and A.S. Abdel-Moneim. 2021. Molecular Docking Reveals Ivermectin and Remdesivir as Potential Repurposed Drugs Against SARS-CoV-2. *Front. Microbiol.* 11. doi:10.3389/fmicb.2020.592908.
- Goddard, T.D., C.C. Huang, E.C. Meng, E.F. Pettersen, G.S. Couch, J.H. Morris, and T.E. Ferrin. 2018. UCSF ChimeraX: Meeting modern challenges in visualization and analysis. *Protein Sci.* 27:14–25. doi:10.1002/pro.3235.
- Grant, T., A. Rohou, and N. Grigorieff. 2018. cisTEM, user-friendly software for single-particle image processing. *Elife*. 7. doi:10.7554/eLife.35383.
- Hanke, L., L. Vidakovics Perez, D.J. Sheward, H. Das, T. Schulte, A. Moliner-Morro, M. Corcoran, A. Achour, G.B. Karlsson Hedestam, B.M. Hällberg, B. Murrell, and G.M. McInerney. 2020. An alpaca nanobody neutralizes SARS-CoV-2 by blocking receptor interaction. *Nat. Commun.* 11:4420. doi:10.1038/s41467-020-18174-5.
- Henderson, R., R.J. Edwards, K. Mansouri, K. Janowska, V. Stalls, S.M.C. Gobeil, M. Kopp, D. Li, R. Parks, A.L. Hsu, M.J. Borgnia, B.F. Haynes, and P. Acharya. 2020. Controlling the SARS-CoV-2 spike glycoprotein conformation. *Nat. Struct. Mol. Biol.* 27:925–933. doi:10.1038/s41594-020-0479-4.
- Hubbard, S.J. and Thornton, J.M. 1993. ‘NACCESS’, computer program. *Dep. Biochem. Mol. Biol. Univ. Coll. London*.
- Huo, J., A. Le Bas, R.R. Ruza, H.M.E. Duyvesteyn, H. Mikolajek, T. Malinauskas, T.K. Tan, P. Rijal, M. Dumoux, P.N. Ward, J. Ren, D. Zhou, P.J. Harrison, M. Weckener, D.K. Clare, V.K. Vogirala, J. Radecke, L. Moynié, Y. Zhao, J. Gilbert-Jaramillo, M.L. Knight, J.A. Tree, K.R. Buttigieg, N. Coombes, M.J. Elmore, M.W. Carroll, L. Carrique, P.N.M. Shah, W. James, A.R. Townsend, D.I. Stuart, R.J. Owens, and J.H. Naismith. 2020. Neutralizing nanobodies bind SARS-CoV-2 spike RBD and block interaction with ACE2. *Nat. Struct. Mol. Biol.* 27:846–854. doi:10.1038/s41594-020-0469-6.
- Ke, Z., J. Oton, K. Qu, M. Cortese, V. Zila, L. McKeane, T. Nakane, J. Zivanov, C.J. Neufeldt, B. Cerikan, J.M. Lu, J. Peukes, X. Xiong, H.-G. Kräusslich, S.H.W. Scheres, R. Bartenschlager, and J.A.G. Briggs. 2020. Structures and distributions of SARS-CoV-2 spike proteins on intact virions. *Nature*. doi:10.1038/s41586-020-2665-2.
- Kirchdoerfer, R.N., C.A. Cottrell, N. Wang, J. Pallesen, H.M. Yassine, H.L. Turner, K.S. Corbett, B.S. Graham, J.S. McLellan, and A.B. Ward. 2016. Pre-fusion structure of a human coronavirus spike protein. *Nature*. 531:118–21. doi:10.1038/nature17200.
- Korber, B., W.M. Fischer, S. Gnanakaran, H. Yoon, J. Theiler, W. Abfalterer, N. Hengartner, E.E. Giorgi, T. Bhattacharya, B. Foley, K.M. Hastie, M.D. Parker, D.G. Partridge, C.M. Evans, T.M. Freeman, T.I. de Silva, C. McDanal, L.G. Perez, H. Tang, A. Moon-Walker, S.P. Whelan, C.C. LaBranche, E.O. Saphire, D.C. Montefiori, A. Angyal, R.L. Brown, L. Carrilero, L.R. Green, D.C. Groves, K.J. Johnson, A.J. Keeley, B.B. Lindsey, P.J. Parsons, M. Raza, S. Rowland-Jones, N. Smith, R.M. Tucker, D. Wang, and M.D. Wyles. 2020. Tracking Changes in SARS-CoV-2 Spike: Evidence that D614G Increases Infectivity of the COVID-19 Virus. *Cell*. 182:812-827.e19. doi:10.1016/j.cell.2020.06.043.
- Kucukelbir, A., F.J. Sigworth, and H.D. Tagare. 2014. Quantifying the local resolution of cryo-EM density maps. *Nat. Methods*. 11:63–5. doi:10.1038/nmeth.2727.
- Lan, J., J. Ge, J. Yu, S. Shan, H. Zhou, S. Fan, Q. Zhang, X. Shi, Q. Wang, L. Zhang, and X. Wang. 2020. Structure of the SARS-CoV-2 spike receptor-binding domain bound to the ACE2 receptor. *Nature*. 581:215–220. doi:10.1038/s41586-020-2180-5.

- Li, F., M. Berardi, W. Li, M. Farzan, P.R. Dormitzer, and S.C. Harrison. 2006. Conformational States of the Severe Acute Respiratory Syndrome Coronavirus Spike Protein Ectodomain. *J. Virol.* 80:6794–6800. doi:10.1128/JVI.02744-05.
- Li, X., P. Mooney, S. Zheng, C.R. Booth, M.B. Braunfeld, S. Gubbens, D.A. Agard, and Y. Cheng. 2013. Electron counting and beam-induced motion correction enable near-atomic-resolution single-particle cryo-EM. *Nat. Methods.* 10:584–590. doi:10.1038/nmeth.2472.
- Liu, J., R. Cao, M. Xu, X. Wang, H. Zhang, H. Hu, Y. Li, Z. Hu, W. Zhong, and M. Wang. 2020. Hydroxychloroquine, a less toxic derivative of chloroquine, is effective in inhibiting SARS-CoV-2 infection in vitro. *Cell Discov.* 6:16. doi:10.1038/s41421-020-0156-0.
- Nimgampalle, M., V. Devanathan, and A. Saxena. 2020. Screening of Chloroquine, Hydroxychloroquine and its derivatives for their binding affinity to multiple SARS-CoV-2 protein drug targets. *J. Biomol. Struct. Dyn.* 1–13. doi:10.1080/07391102.2020.1782265.
- Ou, T., H. Mou, L. Zhang, A. Ojha, H. Choe, and M. Farzan. 2021. Hydroxychloroquine-mediated inhibition of SARS-CoV-2 entry is attenuated by TMPRSS2. *PLOS Pathog.* 17:e1009212. doi:10.1371/journal.ppat.1009212.
- Ou, X., Y. Liu, X. Lei, P. Li, D. Mi, L. Ren, L. Guo, R. Guo, T. Chen, J. Hu, Z. Xiang, Z. Mu, X. Chen, J. Chen, K. Hu, Q. Jin, J. Wang, and Z. Qian. 2020. Characterization of spike glycoprotein of SARS-CoV-2 on virus entry and its immune cross-reactivity with SARS-CoV. *Nat. Commun.* 11:1620. doi:10.1038/s41467-020-15562-9.
- Park, Y.-J., A.C. Walls, Z. Wang, M.M. Sauer, W. Li, M.A. Tortorici, B.-J. Bosch, F. DiMaio, and D. Veasler. 2019. Structures of MERS-CoV spike glycoprotein in complex with sialoside attachment receptors. *Nat. Struct. Mol. Biol.* 26:1151–1157. doi:10.1038/s41594-019-0334-7.
- Pettersen, E.F., T.D. Goddard, C.C. Huang, G.S. Couch, D.M. Greenblatt, E.C. Meng, and T.E. Ferrin. 2004. UCSF Chimera?A visualization system for exploratory research and analysis. *J. Comput. Chem.* 25:1605–1612. doi:10.1002/jcc.20084.
- Pramanick, I., N. Sengupta, S. Mishra, S. Pandey, N. Girish, A. Das, and S. Dutta. 2021. Conformational flexibility and structural variability of SARS-CoV2 S protein. *Structure.* 29:834-845.e5. doi:10.1016/j.str.2021.04.006.
- Repurposed Antiviral Drugs for Covid-19 — Interim WHO Solidarity Trial Results. 2021. *N. Engl. J. Med.* 384:497–511. doi:10.1056/NEJMoa2023184.
- Rohou, A., and N. Grigorieff. 2015. CTFFIND4: Fast and accurate defocus estimation from electron micrographs. *J. Struct. Biol.* 192:216–221. doi:10.1016/j.jsb.2015.08.008.
- Scheres, S.H.W. 2012. RELION: Implementation of a Bayesian approach to cryo-EM structure determination. *J. Struct. Biol.* 180:519–530. doi:10.1016/j.jsb.2012.09.006.
- Tang, G., L. Peng, P.R. Baldwin, D.S. Mann, W. Jiang, I. Rees, and S.J. Ludtke. 2007. EMAN2: An extensible image processing suite for electron microscopy. *J. Struct. Biol.* 157:38–46. doi:10.1016/j.jsb.2006.05.009.
- The PyMOL Molecular Graphics System, Version 1.2r3pre, Schrödinger, LLC.
- Toelzer, C., K. Gupta, S.K.N. Yadav, U. Borucu, A.D. Davidson, M. Kavanagh Williamson, D.K. Shoemark, F. Garzoni, O. Staufer, R. Milligan, J. Capin, A.J. Mulholland, J. Spatz, D. Fitzgerald, I. Berger, and C. Schaffitzel. 2020. Free fatty acid binding pocket in the locked structure of SARS-CoV-2 spike protein. *Science.* doi:10.1126/science.abd3255.
- Tortorici, M.A., and D. Veasler. 2019. Structural insights into coronavirus entry. *Adv. Virus Res.* 105:93–116. doi:10.1016/bs.aivir.2019.08.002.
- Walls, A.C., Y.-J. Park, M.A. Tortorici, A. Wall, A.T. McGuire, and D. Veasler. 2020. Structure, Function, and Antigenicity of the SARS-CoV-2 Spike Glycoprotein. *Cell.*

- 181:281-292.e6. doi:10.1016/j.cell.2020.02.058.
- Warwicker, J. 2020. A model for pH coupling of the SARS-CoV-2 spike protein open/closed equilibrium. *bioRxiv Prepr. Serv. Biol.*
- Wrapp, D., N. Wang, K.S. Corbett, J.A. Goldsmith, C.-L. Hsieh, O. Abiona, B.S. Graham, and J.S. McLellan. 2020. Cryo-EM structure of the 2019-nCoV spike in the prefusion conformation. *Science*. 367:1260–1263. doi:10.1126/science.abb2507.
- Xia, S., Q. Lan, S. Su, X. Wang, W. Xu, Z. Liu, Y. Zhu, Q. Wang, L. Lu, and S. Jiang. 2020. The role of furin cleavage site in SARS-CoV-2 spike protein-mediated membrane fusion in the presence or absence of trypsin. *Signal Transduct. Target. Ther.* 5:92. doi:10.1038/s41392-020-0184-0.
- Xiong, X., K. Qu, K.A. Ciazynska, M. Hosmillo, A.P. Carter, S. Ebrahimi, Z. Ke, S.H.W. Scheres, L. Bergamaschi, G.L. Grice, Y. Zhang, CITIID-NIHR COVID-19 BioResource Collaboration, J.A. Nathan, S. Baker, L.C. James, H.E. Baxendale, I. Goodfellow, R. Doffinger, and J.A.G. Briggs. 2020. A thermostable, closed SARS-CoV-2 spike protein trimer. *Nat. Struct. Mol. Biol.* 27:934–941. doi:10.1038/s41594-020-0478-5.
- Yao, X., F. Ye, M. Zhang, C. Cui, B. Huang, P. Niu, X. Liu, L. Zhao, E. Dong, C. Song, S. Zhan, R. Lu, H. Li, W. Tan, and D. Liu. 2020. In Vitro Antiviral Activity and Projection of Optimized Dosing Design of Hydroxychloroquine for the Treatment of Severe Acute Respiratory Syndrome Coronavirus 2 (SARS-CoV-2). *Clin. Infect. Dis.* 71:732–739. doi:10.1093/cid/ciaa237.
- Yuan, Y., D. Cao, Y. Zhang, J. Ma, J. Qi, Q. Wang, G. Lu, Y. Wu, J. Yan, Y. Shi, X. Zhang, and G.F. Gao. 2017. Cryo-EM structures of MERS-CoV and SARS-CoV spike glycoproteins reveal the dynamic receptor binding domains. *Nat. Commun.* 8:15092. doi:10.1038/ncomms15092.
- Yuan, Z., M.A. Pavel, H. Wang, and S.B. Hansen. 2020. Hydroxychloroquine: mechanism of action inhibiting SARS-CoV2 entry. *bioRxiv Prepr. Serv. Biol.* doi:10.1101/2020.08.13.250217.
- Zhou, P., X.-L. Yang, X.-G. Wang, B. Hu, L. Zhang, W. Zhang, H.-R. Si, Y. Zhu, B. Li, C.-L. Huang, H.-D. Chen, J. Chen, Y. Luo, H. Guo, R.-D. Jiang, M.-Q. Liu, Y. Chen, X.-R. Shen, X. Wang, X.-S. Zheng, K. Zhao, Q.-J. Chen, F. Deng, L.-L. Liu, B. Yan, F.-X. Zhan, Y.-Y. Wang, G.-F. Xiao, and Z.-L. Shi. 2020a. A pneumonia outbreak associated with a new coronavirus of probable bat origin. *Nature*. 579:270–273. doi:10.1038/s41586-020-2012-7.
- Zhou, T., Y. Tsybovsky, J. Gorman, M. Rapp, G. Cerutti, G.-Y. Chuang, P.S. Katsamba, J.M. Sampson, A. Schön, J. Bimela, J.C. Boyington, A. Nazzari, A.S. Olia, W. Shi, M. Sastry, T. Stephens, J. Stuckey, I.-T. Teng, P. Wang, S. Wang, B. Zhang, R.A. Friesner, D.D. Ho, J.R. Mascola, L. Shapiro, and P.D. Kwong. 2020b. Cryo-EM Structures of SARS-CoV-2 Spike without and with ACE2 Reveal a pH-Dependent Switch to Mediate Endosomal Positioning of Receptor-Binding Domains. *Cell Host Microbe*. 28:867-879.e5. doi:10.1016/j.chom.2020.11.004.



(NAYANIKA SENGUPTA)